Dimension-Independent Separate Channel Estimation for RIS-Aided Communications

Chao Jiang, Tianyue Zheng, Jieao Zhu, and Linglong Dai, *Fellow, IEEE*
Department of Electronic Engineering, Tsinghua University,
State Key Laboratory of Space Network and Communications, Beijing 100084, China
Emails: {jiangc24, zhengty22, zja21}@mails.tsinghua.edu.cn, daill@tsinghua.edu.cn

ICC 2026 - IEEE International Conference on Communications | 979-8-3195-4209-0/26/$31.00 ©2026 IEEE | DOI: 10.1109/ICC59461.2026.11586811

***Abstract*—Channel estimation in reconfigurable intelligent surface (RIS) assisted communications requires high pilot overhead due to numerous RIS elements incapable of signal processing. Recently, research on sensing RIS has provided a channel estimation scheme with merely three pilots. Nevertheless, it assumes that the BS-RIS channel is known to RIS and remains invariant over a prolonged period. To address this issue, this paper introduces a generalized approximate message passing (GAMP) based channel estimation framework to achieve dimension-independent estimation of separate channels, without the assumption of known BS-RIS channel. Specifically, we first formulate the channel estimation problem as a compressive phase retrieval problem. Based on phaseless power observations, we leverage the GAMP algorithm to retrieve original sparse signals. Furthermore, by exploiting the intrinsic mapping between the sparse representations of the channels and the power observations in the angular domain, we propose a learned GAMP network to enhance the convergence stability and estimation accuracy. Finally, simulation results demonstrate that the proposed approach can efficiently estimate both the BS-RIS and UE-RIS channels with four pilots.**

***Index Terms*—Reconfigurable intelligent surface (RIS), channel estimation, generalized approximate message passing.**

I. Introduction

Reconfigurable intelligent surface (RIS) has been envisioned as a promising technology due to its capability to reconfigure wireless channels. By properly manipulating the phase-shifts of RIS elements, the reflection signals can be reconfigured to desired directions with high beamforming gain [1]. Fully exploiting this high beamforming gain requires accurate channel state information (CSI), making channel estimation a critical procedure.

Nevertheless, traditional RIS can only reflect the incident signals passively. Therefore, only the cascaded UE-RIS-BS or BS-RIS-UE channel can be estimated at the BS or the UE side. The corresponding dimension of the cascaded channel, given by the product of the number of BS antennas M and the number of RIS elements N, is N times that of the BS-UE channel. To achieve high beamforming gain, RIS is generally fabricated with extremely numerous elements, and the dimension of the cascaded channel increases sharply, resulting in high pilot overhead for channel estimation.

To tackle the above challenge, numerous studies have exploited the structure properties of the cascaded channel. For example, the authors in [2] leveraged the spatial correlation among adjacent RIS elements and divided them into several groups, each configured with common reflection coefficients. Based on this method, the cascaded channel of each group was estimated sequentially with reduced pilot overhead by switching off the other groups. By utilizing the sparsity of channels in the angular domain, researchers in [3], [4] formulated the cascaded channel estimation problem as a compressive sensing (CS) problem, which could be solved by the orthogonal matching pursuit (OMP) algorithm. Additionally, several studies exploited the structure properties that the BS-RIS channel is shared among all users. The authors in [5] first estimated the cascaded channel of a typical user, and then the cascaded channels of the other users are estimated with low pilot overhead based on their strong correlation with that of the typical user. Despite substantial research on low-overhead channel estimation, all the above approaches are designed to estimate the cascaded channel, and the pilot overhead is inevitably proportional to the number of RIS elements.

To further reduce pilot overhead, we have previously conceived a dimension-independent channel estimation approach inspired by optical interference [6], [7]. Specifically, when the signals from the BS and UE are simultaneously transmitted to the RIS, a similar interference random field (IRF) occurs, the power information of which can be exploited to retrieve channel phase information. To capture this power information, a novel hardware architecture named sensing RIS is designed, where each RIS element integrates a low-cost power detector. Based on the power observations, we further proposed a channel estimation framework with dimension-independent pilot overhead [6]. However, this channel estimation approach assumes that the perfect CSI of the BS-RIS channel is known to RIS and remains invariant over a prolonged period, which is impossible in highly dynamic propagation environments.

To resolve the above problems, in this paper, we propose generalized AMP (GAMP) and learned GAMP based channel estimation frameworks to achieve dimension-independent estimation of separate channels. Specifically, inspired by the four-step phase-shift technique in holographic imaging, we formulate the channel estimation problem in sensing RIS systems as a compressive phase retrieval problem. By designing a block-structured sensing matrix, the BS–RIS and UE–RIS channels contribute to the power observations in a distinguishable manner, thus enabling individual estimation of the two separate channels. Then, we leverage the GAMP algorithm to develop a practical channel estimation scheme. This scheme does not require the assumption that the BS-RIS channel is known, and achieves accurate channel estimation with only four pilots. Furthermore, we propose a learned GAMP algorithm that capitalizes on the intrinsic mapping between sparse representations of the channels and the IRF. We develop an initial-value network for parameter initialization and transform the fixed damping coefficient into trainable parameters, significantly enhancing the algorithm's convergence and accuracy. Finally, simulation results demonstrate that the proposed approach can efficiently estimate both the BS-RIS and UE-RIS channels.

II. System Model for Sensing RIS

A. Channel Model

We consider a RIS-aided wireless communication system, in which one user equipment (UE) is served by a base station (BS) with the assistance of RIS with N elements. To simplify the design and analysis of the algorithms, it is assumed that the direct line-of-sight (LoS) BS-UE link is blocked and both the BS and the UE have a single-antenna. Let $\mathbf{g} \in \mathbb{C}^N$ ($\mathbf{f} \in \mathbb{C}^N$) denote the channel from the BS (UE) to the RIS, respectively. The multipath Saleh-Valenzuela channel model can be employed to characterize $\mathbf{g}$ as

$$\mathbf{g} = \sqrt{\frac{N}{L_g}} \sum_{\ell_1=0}^{L_g-1} \alpha_{\ell_1}^g \mathbf{a}(\theta_{\ell_1}^g, \phi_{\ell_1}^g), \tag{1}$$

where $\alpha_{\ell_1}^g$ and $\theta_{\ell_1}^g$ ($\phi_{\ell_1}^g$) denotes the complex path gain and the azimuth (elevation) angle of the ℓ_1-th path, respectively. Similarly, the UE-RIS channel $\mathbf{f}$ is given by

$$\mathbf{f} = \sqrt{\frac{N}{L_f}} \sum_{\ell_2=0}^{L_f-1} \alpha_{\ell_2}^f \mathbf{a}(\theta_{\ell_2}^f, \phi_{\ell_2}^f), \tag{2}$$

where $\alpha_{\ell_2}^f$ and $\theta_{\ell_2}^f$ ($\phi_{\ell_2}^f$) denotes the complex path gain and the azimuth (elevation) angle of the ℓ_2-th path. $\mathbf{a}(\theta, \phi) \in \mathbb{C}^N$ represents the normalized array steering vector for the RIS. Given a typical UPA with $N = N_1 \times N_2$ elements, $\mathbf{a}(\theta, \phi)$ can be represented as $\mathbf{a}(\theta, \phi) = \frac{1}{\sqrt{N}} \left[e^{-j2\pi d \sin(\theta)\cos(\phi)\mathbf{n}_1/\lambda}\right] \otimes \left[e^{-j2\pi d \sin(\phi)\mathbf{n}_2/\lambda}\right]$, where $\mathbf{n}_1 = [0, 1, \cdots, N_1 - 1]^T$ and $\mathbf{n}_2 = [0, 1, \cdots, N_2 - 1]^T$, λ denotes the carrier wavelength, and d is the antenna spacing satisfying $d = \lambda/2$.

Furthermore, assuming that both $\mathbf{g}$ and $\mathbf{f}$ are sparse in the angular domain, $\mathbf{g}$ and $\mathbf{f}$ can be represented in the angular domain as $\mathbf{g} = \mathbf{U}\tilde{\mathbf{g}}$, $\mathbf{f} = \mathbf{U}\tilde{\mathbf{f}}$, where $\tilde{\mathbf{g}} \in \mathbb{C}^N$ and $\tilde{\mathbf{f}} \in \mathbb{C}^N$ are sparse angular-domain representations. Besides, the codebook $\mathbf{U} \in \mathbb{C}^{N \times N}$ is defined to be

$$\begin{aligned}\mathbf{U} = \big[&\bar{\mathbf{a}}(\bar{\theta}_1, \bar{\phi}_1) \cdots, \bar{\mathbf{a}}(\bar{\theta}_1, \bar{\phi}_{N_2}), \cdots, \\ &\bar{\mathbf{a}}(\bar{\theta}_{N_1}, \bar{\phi}_1) \cdots, \bar{\mathbf{a}}(\bar{\theta}_{N_1}, \bar{\phi}_{N_2})\big],\end{aligned} \tag{3}$$

where the spatial angles of azimuth and elevation are represented as $\bar{\theta}_n = \frac{2}{N_1}(n - \frac{N_1+1}{2}), n = 1, 2, \cdots, N_1$ and $\bar{\phi}_n = \frac{2}{N_2}(n - \frac{N_2+1}{2}), n = 1, 2, \cdots, N_2$. The codebook atoms $\bar{\mathbf{a}}(\bar{\theta}, \bar{\phi})$ can be presented by $\bar{\mathbf{a}}(\bar{\theta}, \bar{\phi}) = \frac{1}{\sqrt{N}}[e^{-j\pi\bar{\theta}\mathbf{n}_1}] \otimes [e^{-j\pi\bar{\phi}\mathbf{n}_2}]$.

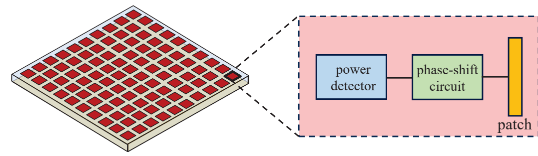

Fig. 1. Sensing RIS hardware architecture.

B. Signal Model

Given the channel model, the received signal of the UE can be represented as

$$y_{\mathrm{UE}} = \sqrt{P_{\mathrm{BS}}}\mathbf{f}^H \mathbf{\Psi} \mathbf{g} s + v, \tag{4}$$

where P_{BS} is the transmitting power of the BS; s denotes the normalized BS transmitting symbol; $\mathbf{\Psi} = \mathrm{diag}(\boldsymbol{\psi}) = \mathrm{diag}([\psi_1, \cdots, \psi_N]^T)$ is the RIS phase-shift matrix with $\psi_n \in \mathbb{C}$, $|\psi_n| = 1$ representing the phase-shift of the n-th RIS element; $v \sim \mathcal{CN}(0, \nu^v)$ is the received thermal noise introduced at the UE. If the channels $\mathbf{g}$ and $\mathbf{f}$ are known, then we can easily obtain the RIS phase-shift matrix $\mathbf{\Psi}$ as $\psi_n^{\mathrm{opt}} = \exp(-j\arg(g_n f_n^*))$. However, due to the rapid changing of the wireless environment, these channel vectors require frequent re-estimation, causing unaffordable pilot overhead in traditional RIS assisted communications.

To address this problem, we replace the conventional passive RIS with a sensing RIS [6]. Compared with traditional RIS as a phase-shift circuit, sensing RIS elements additionally integrate power detectors to capture the IRF signal, as shown in Fig. 1. The detected signal $\mathbf{p} \in \mathbb{R}_{\geq 0}^N$ can be defined as

$$\mathbf{p} = \left|\sqrt{P_{\mathrm{BS}}}\mathbf{g}s + \sqrt{P_{\mathrm{UE}}}\mathbf{f}s' + \mathbf{w}\right|^2 \odot \mathrm{vec}(\mathcal{H}). \tag{5}$$

where $\mathbf{w} \sim \mathcal{CN}(\mathbf{0}, \nu^w \mathbf{I}_N)$ represents the noise introduced in the power detectors, and $\mathcal{H} \in \{0, 1\}^{N_1 \times N_2}$ denotes the positions of N_s power detectors, which is defined as

$$\mathcal{H}_{k,\ell} = \begin{cases} 1, & \text{power detector present at } (k, \ell) \\ 0, & \text{otherwise.} \end{cases} \tag{6}$$

C. Problem Formulation

Estimating the separate channels of BS-RIS and UE-RIS, is equivalent to reconstructing the sparse signal $\mathbf{x} = [\sqrt{P_{\mathrm{BS}}}\tilde{\mathbf{f}}^T, \sqrt{P_{\mathrm{UE}}}\tilde{\mathbf{g}}^T]^T$ from the power observations, which can be regarded as a compressive phase retrieval problem. Inspired by the four-step phase-shift methodology in holographic imaging, which can extract phase information from $Q = 4$ exposures by imposing different phase-shifts to one optical path, we can construct the sensing matrix $\mathbf{A} \in \mathbb{C}^{4N_s \times 2N}$ as

$$\mathbf{A} = \begin{bmatrix} \mathbf{U}_{\mathcal{H}} & \mathbf{O}_{N_s \times N} \\ \mathbf{O}_{N_s \times N} & \mathbf{U}_{\mathcal{H}} \\ \mathbf{U}_{\mathcal{H}} & j\mathbf{U}_{\mathcal{H}} \\ \mathbf{U}_{\mathcal{H}} & \mathbf{U}_{\mathcal{H}} \end{bmatrix}, \tag{7}$$

where $\mathbf{O}_{N_s \times N}$ denotes the all-zero matrix of size $N_s \times N$, and $\mathbf{U}_{\mathcal{H}}$ characterizes the row-wise selection mechanism determined by the non-zero entries of $\mathrm{vec}(\mathcal{H})$.

Since the estimated sparse signal $\mathbf{x}$ needs to simultaneously satisfy the IRF observation equation and the sparsity prior, an optimization problem can be formulated as

$$\min_{\mathbf{x}} \ \mathcal{L}(\mathbf{x}) = \frac{1}{2}\left\|\mathbf{y} - |\mathbf{A}\mathbf{x}|\right\|_2^2 + \lambda \left\|\mathbf{x}\right\|_1, \tag{8}$$

where λ denotes the regularization factor balancing prior knowledge on sparsity and error of solution, and the received magnitude signal $\mathbf{y} \in \mathbb{R}_{\geq 0}^{4N_s}$ can be expressed as $\mathbf{y} = [\sqrt{\mathbf{p}}_{1,\mathcal{H}}^T, \sqrt{\mathbf{p}}_{2,\mathcal{H}}^T, \sqrt{\mathbf{p}}_{3,\mathcal{H}}^T, \sqrt{\mathbf{p}}_{4,\mathcal{H}}^T]^T$. If the noncoherent sparse recovery problem (8) can be solved efficiently, then the separate channels $\tilde{\mathbf{f}}$ and $\tilde{\mathbf{g}}$ can be acquired. Unfortunately, due to the absolute term $|\mathbf{A}\mathbf{x}|$, the problem is highly non-convex.

III. Proposed Channel Estimation Scheme via GAMP Algorithm

A. Preliminaries of GAMP Algorithm

Various methods can be applied to resolve the compressive phase retrieval problem. Among these methods, GAMP algorithm [8] has emerged as a prominent solution, demonstrating remarkable efficiency and robustness. GAMP is an iterative Bayesian inference algorithm. As an extension of the standard AMP framework, GAMP algorithm can incorporate arbitrary input and output distributions, and is applicable to linear as well as nonlinear observation models.

Focusing on problem (8), if the posterior distribution $p(\mathbf{x}|\mathbf{y})$ can be available, we can implement maximum a posteriori (MAP) and minimum mean square error (MMSE) estimation. However, the true posterior distribution $p(\mathbf{x}|\mathbf{y})$ is analytically intractable and computationally prohibitive. To address this problem, the GAMP algorithm performs loopy belief propagation (BP) on a factor graph. Specifically, assuming that the components of the unknown vector $\mathbf{x}$ are statistically independent, we can factorize the posterior distribution as

$$p(\mathbf{x}|\mathbf{y}) \propto p(\mathbf{y}|\mathbf{x})p(\mathbf{x}) = \prod_m p(y_m|z_m)\prod_n p(x_n), \tag{9}$$

where $\mathbf{z} \triangleq \mathbf{A}\mathbf{x}$ denotes a linear transform. Then the factors of $p(\mathbf{x}|\mathbf{y})$ are represented as factor nodes and each x_n constitutes variable nodes in the factor graph. Through message passing between these nodes, the estimation of $\mathbf{x}$ is iteratively updated until all nodes converge towards a consensus.

B. Recover Full Channels from Sampled IRF

This subsection will present how to leverage the GAMP algorithm to recover sparse signal $\mathbf{x}$ from phaseless observations $\mathbf{y}$, as summarized in **Algorithm** 1.

The output nonlinear functions $g_{\text{out}}(\cdot)$ and $g'_{\text{out}}(\cdot)$ in lines 7 and 8 of **Algorithm 1** are defined as

$$\begin{aligned} g_{\text{out}}(y_m, \hat{p}_m, \nu_m^p) &= \left(\mathbb{E}\left[z_m|y_m;\hat{p}_m,\nu_m^p\right] - \hat{p}_m\right)/\nu_m^p, \\ g'_{\text{out}}(y_m, \hat{p}_m, \nu_m^p) &= \left(\text{var}\left[z_m|y_m;\hat{p}_m,\nu_m^p\right] - \nu_m^p\right)/(\nu_m^p)^2. \end{aligned} \tag{10}$$

Since $\mathbf{y} = |\mathbf{z} + \mathbf{w}|$, $y_m|z_m$ follows a Rician distribution $p(y_m|z_m) = \frac{2y_m}{\nu^w}\exp(-\frac{y_m^2+|z_m|^2}{\nu^w})I_0(\frac{2y_m|z_m|}{\nu^w})$, where $I_0(\cdot)$ is the zeroth-order modified Bessel function of the first kind.

Algorithm 1 Sum-Product GAMP Algorithm

Input: Sparse sensing matrix $\mathbf{A} \in \mathbb{C}^{4N_s \times 2N}$, observed amplitude signal $\mathbf{y} \in \mathbb{R}_{\geq 0}^{4N_s}$, precision tolerance ϵ, maximum number of iterations $T_{\max}$.

Ouput: Estimated sparse signal $\mathbf{x} \in \mathbb{C}^{2N}$.

1: $\mathbf{B} = \text{abs}(\mathbf{A})^2$
2: **repeat**
3: $\quad \boldsymbol{\nu}^p(t) = \beta\mathbf{B}\boldsymbol{\nu}^x(t) + (1-\beta)\boldsymbol{\nu}^x(t-1)$
4: $\quad \alpha(t) = \text{mean}(\boldsymbol{\nu}^p(t))$
5: $\quad \hat{\mathbf{p}}(t) = \mathbf{A}\hat{\mathbf{x}}(t) - \frac{1}{\alpha(t)}\boldsymbol{\nu}^p(t) \odot \hat{\mathbf{s}}(t-1)$
6: $\quad \hat{\mathbf{s}}(t) = \beta g_{\text{out}}(\mathbf{y}, \hat{\mathbf{p}}(t), \boldsymbol{\nu}^p(t)) + (1-\beta)\hat{\mathbf{s}}(t-1)$
7: $\quad \boldsymbol{\nu}^s(t) = (1-\beta)\boldsymbol{\nu}^s(t-1) - \beta\alpha(t)g'_{\text{out}}(\mathbf{y}, \hat{\mathbf{p}}(t), \boldsymbol{\nu}^p(t))$
8: $\quad \boldsymbol{\nu}^r(t) = \left(\mathbf{B}^T\boldsymbol{\nu}^s(t)\right)^{-1}$
9: $\quad \hat{\mathbf{r}}(t) = \hat{\mathbf{x}}(t) + \boldsymbol{\nu}^r(t) \odot \left(\mathbf{A}^H\hat{\mathbf{s}}(t)\right)$
10: $\quad \bar{\mathbf{x}}(t) = \beta\hat{\mathbf{x}}(t) + (1-\beta)\bar{\mathbf{x}}(t-1)$
11: $\quad \boldsymbol{\nu}^x(t+1) = \alpha(t)\boldsymbol{\nu}^r(t) \odot g'_{\text{in}}(\hat{\mathbf{r}}(t), \alpha(t)\boldsymbol{\nu}^r(t))$
12: $\quad \hat{\mathbf{x}}(t+1) = g_{\text{in}}(\hat{\mathbf{r}}(t), \alpha(t)\boldsymbol{\nu}^r(t))$
13: $\quad t \leftarrow t+1$
14: **until** $t > T_{\max}$ or $\|\hat{\mathbf{x}}(t+1) - \bar{\mathbf{x}}(t)\|^2 < \epsilon$

Moreover, through the central limit theorem, GAMP algorithm approximates z_m following a Gaussian distribution with mean $\hat{p}_m$ and variance ν_m^p. Then the marginal posterior distribution $p(z_m|y_m;\hat{p}_m,\nu_m^p)$ can be approximated as

$$p(z_m|y_m;\hat{p}_m,\nu_m^p) = \frac{p(y_m|z_m)\mathcal{CN}(z_m;\hat{p}_m,\nu_m^p)}{\int p(y_m|z_m)\mathcal{CN}(z_m;\hat{p}_m,\nu_m^p)dz_m}. \tag{11}$$

Thus, the conditional mean and variance of $z_m|y_m$ are readily available, as derived in [8]

$$\begin{aligned} \mathbb{E}\left[z_m|y_m;\hat{p}_m,\nu_m^p\right] &= \left(\frac{y_m R_0(\varrho_m)}{1+\nu^w/\nu_m^p} + \frac{|\hat{p}_m|}{1+\nu_m^p/\nu^w}\right)\frac{\hat{p}_m}{|\hat{p}_m|}, \\ \text{var}\left[z_m|y_m;\hat{p}_m,\nu_m^p\right] &= \frac{y_m^2}{(1+\nu^w/\nu_m^p)^2} + \frac{|\hat{p}_m|^2}{(1+\nu_m^p/\nu^w)^2} + \\ &\quad \frac{1+\varrho_m R_0(\varrho_m)}{1/\nu^w + 1/\nu_m^p} - \left|\mathbb{E}\left[z_m|y_m;\hat{p}_m,\nu_m^p\right]\right|^2, \end{aligned} \tag{12}$$

where $R_0(\varrho_m) \triangleq \frac{I_1(\varrho_m)}{I_0(\varrho_m)}$ and $\varrho_m \triangleq \frac{2y_m|\hat{p}_m|}{\nu^w+\nu_m^p}$.

To derive the specific expressions of the input nonlinear functions $g_{\text{in}}(\cdot)$ and $g'_{\text{in}}(\cdot)$, we assume that $\mathbf{x}$ is known to be K-sparsity but lacks prior information on its support. Then, the Bernoulli-Gaussian (BG) model is conventionally adopted

$$p(x_n) = (1-\kappa)\delta(x_n) + \kappa\mathcal{CN}(x_n;0,\sigma_x^2), \tag{13}$$

where $\kappa \triangleq K/N$ denotes sparsity rate and σ_x^2 is the variance. For this prior, the input nonlinear functions can be denoted as

$$
\begin{aligned}
g_{\mathrm{in}}(\hat{r}_n, \nu_n^r) &= \mathbb{E}\left[x_n | \hat{r}_n; \nu_n^r\right] = \frac{\xi_n}{1+\eta_n e^{-\zeta_n |\hat{r}_n|^2}}, \\
g_{\mathrm{in}}'(\hat{r}_n, \nu_n^r) &= \frac{\nu_n^r \xi_n (1+\zeta_n |\hat{r_n}|^2)}{1+\eta_n e^{-\zeta_n |\hat{r_n}|^2}} - \left|\mathbb{E}\left[x_n | \hat{r}_n; \nu_n^r\right]\right|^2,
\end{aligned} \tag{14}
$$

where $\xi_n \triangleq \frac{\sigma_x^2}{\nu_n^r+\sigma_x^2}$, $\eta_n \triangleq \frac{1-\kappa}{\kappa}\frac{\nu_n^r+\sigma_x^2}{\nu_n^r}$, and $\zeta_n \triangleq \frac{\sigma_x^2}{\nu_n^r(\nu_n^r+\sigma_x^2)}$.

To enhance convergence of the algorithm, a damping factor $\beta \in (0,1]$ is incorporated to regulate the iterative variables updates, leading to a trade-off between guaranteed convergence and reduced convergence speed. Note that through numerous experiments, β is typically configured to be 0.25 [8].

IV. Proposed Learned GAMP Network for Channel Estimation

A. Challenges of GAMP Algorithm

Although GAMP algorithm achieves remarkable efficiency in phase retrieval problems, its practical applications face inherent limitations, particularly severe in our problem.

First, GAMP algorithm is susceptible to convergence at local minima, leading to large reconstruction errors, especially when the sensing matrix is ill-conditioned or the sparsity of the signal is not guaranteed strictly. To avoid bad local minima, the most typically adopted solution is implementing multiple random initializations, restarting repeatedly, and selecting the best result as the final output [8]. Although repeated experiments can enhance convergence and accuracy, the time complexity is unacceptable for future communications.

Besides, another critical drawback is the configuration of the damping factor β. Specifically, the theoretical determination of an optimal damping factor is challenging in existing algorithm architecture. Therefore, the damping factor is conventionally set to an empirical value 0.25, rather than an optimized value for the specific problem. Moreover, the identical damping factor across all variable updates leads to a significant limitation, which disregards the heterogeneous convergence dynamics of different variables.

To address these drawbacks, we develop a learned GAMP algorithm that capitalizes on the properties of IRF as follows.

B. IRF Spectrum Analysis

In order to retrieve the channel matrix, we need to exploit the structural properties of $\mathbf{p}$. Due to the sparsity of channel in the angular domain, the IRF signals also exhibit sparsity. Moreover, the indices of non-zero elements of $\tilde{\mathbf{g}}$ and $\tilde{\mathbf{f}}$ have a relationship with those of the sparse representation of $\mathbf{p}$.

Here we firstly derive the relationship between the power signal $\mathbf{p}$ and the original phased $\mathbf{q} \triangleq \sqrt{P_{\mathrm{BS}}}\mathbf{g}s + \sqrt{P_{\mathrm{UE}}}\mathbf{f}s' + \mathbf{v}$.

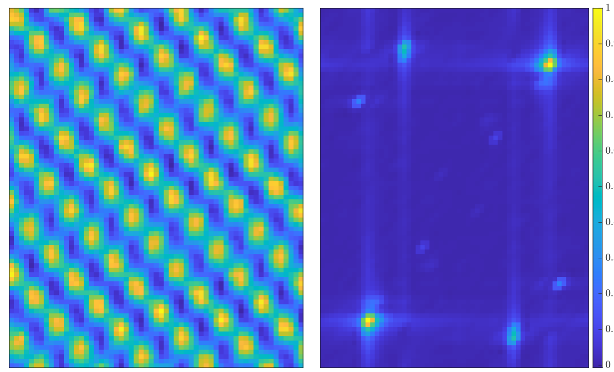

(a) Spatial domain. (b) Angular domain.

Fig. 2. Normalized IRF pattern in the spatial (angular) domain.

We construct $\mathbf{Q} \in \mathbb{C}^{N_1 \times N_2}$, $\mathbf{P} \in \mathbb{R}_{\geq 0}^{N_1 \times N_2}$, satisfying $\mathbf{q} = \mathrm{vec}(\mathbf{Q})$, $\mathbf{p} = \mathrm{vec}(\mathbf{P})$. Since $\mathbf{P} = \mathbf{Q} \odot \mathbf{Q}^*$, it follows that

$$
\begin{aligned}
\hat{\mathbf{P}}_{k1,k2} &= \frac{1}{N}\left(\hat{\mathbf{Q}} \star \widehat{\mathbf{Q}^*}\right)_{k_1,k_2} \\
&= \frac{1}{N}\sum_{n_2=0}^{N_2-1}\sum_{n_1=0}^{N_1-1} \hat{\mathbf{Q}}_{n_1,n_2} \hat{\mathbf{Q}}^*_{\left((n_1-k_1)\right)_{N_1}, \left((n_2-k_2)\right)_{N_2}} \\
&= \frac{1}{N}\left(\mathbf{R}_{\hat{\mathbf{Q}},\hat{\mathbf{Q}}}\right)_{k_1,k_2},
\end{aligned} \tag{15}
$$

where $\hat{\mathbf{P}}$ denotes the 2D-DFT of $\mathbf{P}$, $\star$ denotes circular convolution operation, and $\mathbf{R}_{\mathbf{A},\mathbf{B}}$ represents the correlation matrix. Equation (15) demonstrates that the 2D-DFT of the non-coherent signal $\mathbf{P}$ is the autocorrelation matrix of the spectrum of the coherent signal $\mathbf{q}$. To simplify analysis, we consider that both the BS-RIS channel and UE-RIS channel are single-path channels firstly, and then extend the analysis to multi-path scenario. By assuming an on-grid incident angle, the received coherent signal $\mathbf{q}$ is given by

$$
\mathbf{q} = \sqrt{P_{\mathrm{BS}}}\alpha^g \mathbf{f}_{N_1,\ell_1} \otimes \mathbf{f}_{N_2,\ell_2} + \sqrt{P_{\mathrm{UE}}}\alpha^f \mathbf{f}_{N_1,\ell_1'} \otimes \mathbf{f}_{N_2,\ell_2'}, \tag{16}
$$

where $\mathbf{f}_{N,\ell}$ denotes the ℓ-th column of the $N \times N$ DFT matrix. Thus, the spectrum of $\mathbf{Q} = \mathrm{unvec}(\mathbf{q})$ is given by

$$
\hat{\mathbf{Q}} = \sqrt{P_{\mathrm{BS}}}\alpha^g \mathbf{e}_{\ell_1}\mathbf{e}_{\ell_2}^T + \sqrt{P_{\mathrm{UE}}}\alpha^f \mathbf{e}_{\ell_1'}\mathbf{e}_{\ell_2'}^T \triangleq \mathbf{Q}_1 + \mathbf{Q}_2, \tag{17}
$$

where $\mathbf{e}_\ell$ denotes the unit vector with the only non-zero element in its ℓ-th entry. According to (15), the autocorrelation matrix of $\hat{\mathbf{Q}}$ is then given by

$$
\begin{aligned}
R_{\hat{\mathbf{Q}},\hat{\mathbf{Q}}} =& R_{\hat{\mathbf{Q}}_1,\hat{\mathbf{Q}}_1} + R_{\hat{\mathbf{Q}}_1,\hat{\mathbf{Q}}_2} + R_{\hat{\mathbf{Q}}_2,\hat{\mathbf{Q}}_1} + R_{\hat{\mathbf{Q}}_2,\hat{\mathbf{Q}}_2} \\
=& (P_{\mathrm{BS}}|\alpha^g|^2 + P_{\mathrm{UE}}|\alpha^f|^2)\mathbf{e}_0\mathbf{e}_0^T \\
&+ \sqrt{P_{\mathrm{BS}}P_{\mathrm{UE}}}\alpha^g {\alpha^f}^* \mathbf{e}_{\left((\ell_1-\ell_1')\right)_{N_1}} \mathbf{e}^T_{\left((\ell_2-\ell_2')\right)_{N_2}} \\
&+ \sqrt{P_{\mathrm{BS}}P_{\mathrm{UE}}}{\alpha^g}^* \alpha^f \mathbf{e}_{\left((\ell_1'-\ell_1)\right)_{N_1}} \mathbf{e}^T_{\left((\ell_2'-\ell_2)\right)_{N_2}}.
\end{aligned} \tag{18}
$$

Therefore, the spectrum of the IRF signal exhibits a triple-peak pattern, with one peak $\mathbf{e}_0\mathbf{e}_0^T$ located at the zero-frequency origin, and another two conjugate-symmetric peaks located at the "difference frequency". The "difference frequency" corresponds to difference of incident angles of UE-RIS and BS-RIS beams. Thus, the indices of these two peaks are related to the indices of non-zero entries in $\tilde{\mathbf{g}}$ and $\tilde{\mathbf{f}}$. Then we consider multi-path scenarios. A general multipath IRF with L_g BS-RIS paths and L_f UE-RIS paths will exhibits $(L_g+L_f)(L_g+L_f-1)+1$ peaks, as shown in Fig. 2. Similarly, these peaks also contain the information of $\tilde{\mathbf{g}}$ and $\tilde{\mathbf{f}}$.

C. Deep Learning Based Model Design

As discussed in Subsection IV-B, the IRF spectrum is highly connected to the sparse signal $\mathbf{x}$. Thus, we aim to strategically leverage the insight to resolve the inherent limitations of GAMP algorithm. Specifically, the IRF signal demonstrates sparsity in the angular domain, with its non-zero indices mapped to the support set of $\mathbf{x}$, which can be expressed as

$$\mathcal{M}: \ \mathrm{supp}(\hat{\mathbf{P}}) \rightarrow \mathrm{supp}(\mathbf{x}), \tag{19}$$

where $\mathrm{supp}(\cdot)$ denotes the support set of a sparse vector or matrix. Therefore, it is feasible to exploit the properties of $\mathbf{x}$ and IRF in the angular domain, to provide effective initialization for GAMP algorithm. However, the aforementioned mapping $\mathcal{M}$ lacks mathematical characterization in multi-path scenarios, particularly when the number of paths is large. To overcome this issue, deep learning can be leveraged to extract features and fit the intricate nonlinear mapping through data-driven approach [9]. Hence, we utilize neural network to acquire effective initialization for enhanced algorithmic convergence, with its specific structure depicted in Fig. 3.

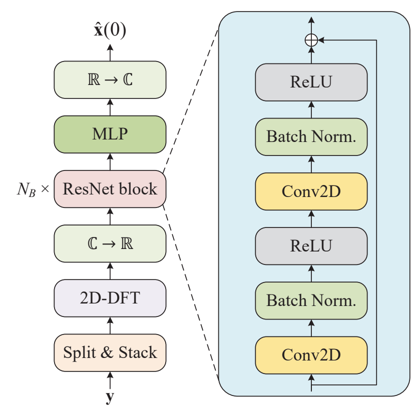

Fig. 3. Specific network structure of the designed initializer.

The network takes as input the IRF signal $\mathbf{y}$, which is constructed by concatenating $Q = 4$ pilot observations and undergoes a pre-processing step labeled as "Split & Stack". This operation reorganizes the input into a format suitable for further transformation. Subsequently, to capture angular domain characteristics and fit the mapping $\mathcal{M}$, we apply 2D-DFT to convert to the angular domain. To be compatible with traditional real-valued neural network, the complex-valued signal is decomposed into real and imaginary components. Further, the resulting real-valued signal is passed through N_B cascaded residual blocks to extract multi-scale features. Each residual block comprises two convolutional layers, followed by batch normalization and ReLU activation function, without incurring large number of parameters. Then the multi-scale feature maps are processed via a multilayer perceptron (MLP), which serves as a global feature integrator. The MLP output is subsequently converted back to the complex domain, and $\hat{\mathbf{x}}(0)$ is regarded as an efficient initial value of GAMP algorithm.

To address the latter limitation, the classical GAMP algorithm is deep unfolded into a neural network. The damping factors, traditionally regarded as empirically chosen hyperparameters, are redefined as trainable parameters. This configuration enables the model to learn optimal damping factors directly from data during the training process, thereby enhancing adaptability and convergence performance. In particular, the damping factors are not uniform across layers, such that each layer maintains its own distinct set of damping factors.

To construct a fully learnable architecture, the initializer is integrated into the deep unfolded neural network, resulting in a unified framework wherein both components are jointly optimized. The loss function is defined in (8), enabling end-to-end training of all parameters through gradient-based optimization.

V. Simulation Results and Discussion

In our simulation experiments, the system model described in Section II is considered. The number of RIS elements is $N = 32 \times 16$, the carrier frequency is 3.5 GHz, and the numbers of BS-RIS and UE-RIS paths are configured to $L_g = L_f = 4$. The azimuth and elevation angles are randomly sampled from the uniform distribution $\mathcal{U}(-\pi/2, \pi/2)$. The complex channel gains $\alpha^g \sim \mathcal{CN}(0, \lambda^2/(4\pi R_{\mathrm{BS}})^2)$ and $\alpha^f \sim \mathcal{CN}(0, \lambda^2/(4\pi R_{\mathrm{UE}})^2)$, where $R_{\mathrm{BS}}(R_{\mathrm{UE}})$ represents the distance between the BS (UE) and the RIS. To quantify the signal quality at the RIS and compare performances of different channel estimation schemes, we define the interferential SNR as $\bar{\gamma} \triangleq (\frac{P_{\mathrm{BS}}\lambda^2}{(4\pi R_{\mathrm{BS}})^2} + \frac{P_{\mathrm{UE}}\lambda^2}{(4\pi R_{\mathrm{UE}})^2})\frac{1}{\nu^w}$.

The CSI acquisition accuracy of different channel estimation schemes is exhibited in Fig. 4 and Fig. 5. In the simulation of the proposed GAMP-based channel estimation method, the number of random initializations N_t is set to 1, 2, and 4. In addition, we consider the "LS-Oracle" scheme as our benchmark, where the supports of the sparse channels and the phases of the IRF signals are assumed to be known. From the simulation results in Fig. 4 and Fig. 5, the proposed GAMP-based framework enables accurate separate channel estimation with merely 4 pilots, regardless of the number of RIS elements, thus achieving dimension-independent separate channel estimation. Regarding the learned GAMP algorithm, it consistently outperforms GAMP across almost all interferential SNR levels. It is worth noting that, the NMSE of the GAMP algorithm does not decrease monotonically with increasing SNR, primarily because the algorithm exhibits an oscillatory convergence behavior against interferential SNR. This can be due to that, in moderate-to-high interferential SNR regions, the presence of non i.i.d Gaussian measurement

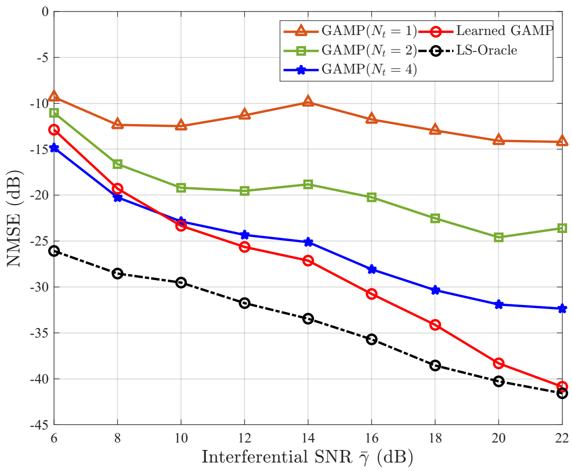

Fig. 4. NMSE of the BS-RIS channel estimators.

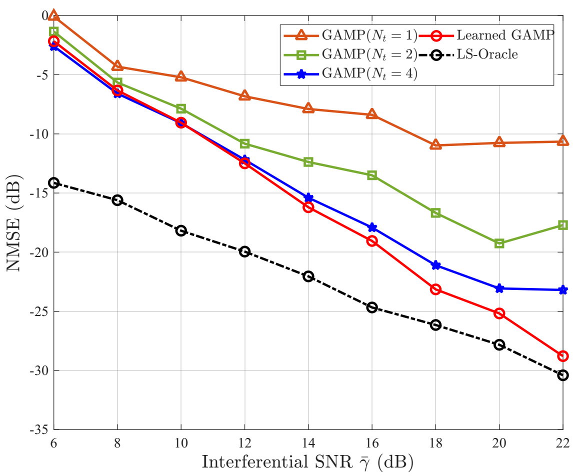

Fig. 5. NMSE of the UE-RIS channel estimators.

matrix exacerbates the failure of "Onsager correction" term in GAMP algorithm, leading to frequent divergence [10].

Fig. 6 exhibits the convergence of the conventional GAMP and learned GAMP algorithm using the cumulative distribution function (CDF) of NMSE. The learned GAMP network converges to a NMSE($\mathbf{g}$) below -30 dB in nearly 90 percent and a NMSE($\mathbf{f}$) below -20 dB in 85 percent of the trials, while the traditional GAMP achieves the same NMSE in only 30 percent. These results demonstrate the reliable convergence advantage of the learned GAMP algorithm. This improvement can be attributed to: 1) The learnable initializer provides an intial value close to the global optimum based on the intrinsic connection between sparse representations of the channels and the IRF in the angular domain; 2) layer-wise trainable damping factors adaptively regulate message passing and adjust variable update dynamics to avoid poor local minima. Therefore, the learned GAMP framework mitigates convergence to poor local minima and even divergency, making it a practical and scalable solution to real-time and high-accuracy channel estimation.

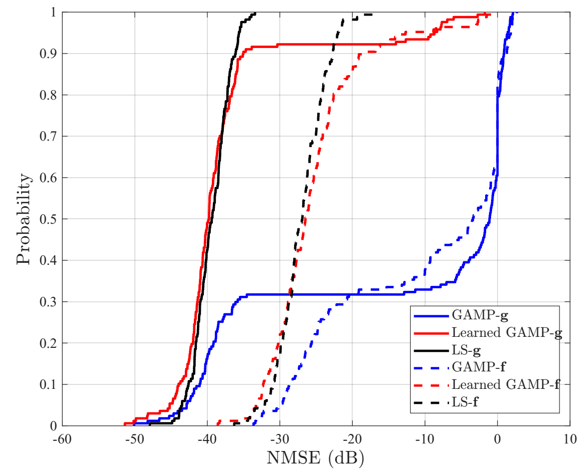

Fig. 6. CDF of NMSE. The interferential SNR $\bar{\gamma} = 20$ dB.

VI. Conclusion

In this study, RIS channel estimation problem has been formulated as a compressive phase retrieval problem, and a GAMP based channel estimation method has been proposed. The method achieves dimension-independent estimation of separate BS-RIS and UE-RIS channels utilizing four pilots. Furthermore, by exploiting the sparsity of the IRF in the angular domain, we have designed a learned GAMP network to enhance the algorithm's convergence and estimation accuracy.

Acknowledgment

This work was funded by the National Science Fund for Distinguished Young Scholars (Grant No. 62325106).

References

[1] Q. Wu and R. Zhang, "Intelligent reflecting surface enhanced wireless network via joint active and passive beamforming," *IEEE Trans. Wireless Commun.*, vol. 18, no. 11, pp. 5394–5409, Nov. 2019.

[2] Y. Yang, B. Zheng, S. Zhang, and R. Zhang, "Intelligent reflecting surface meets OFDM: Protocol design and rate maximization," *IEEE Trans. Commun.*, vol. 68, no. 7, pp. 4522–4535, Jul. 2020.

[3] P. Wang, J. Fang, H. Duan, and H. Li, "Compressed channel estimation for intelligent reflecting surface-assisted millimeter wave systems," *IEEE Signal Process. Lett.*, vol. 27, pp. 905–909, May 2020.

[4] T. Lin, X. Yu, Y. Zhu, and R. Schober, "Channel estimation for IRS-assisted millimeter-wave MIMO systems: Sparsity-inspired approaches," *IEEE Trans. Commun.*, vol. 70, no. 6, pp. 4078–4092, Jun. 2022.

[5] G. Zhou, C. Pan, H. Ren, P. Popovski, and A. L. Swindlehurst, "Channel estimation for RIS-aided multiuser millimeter-wave systems," *IEEE Trans. Signal Process.*, vol. 70, pp. 1478–1492, Mar. 2022.

[6] J. Zhu, K. Liu, Z. Wan, L. Dai, T. J. Cui, and H. V. Poor, "Sensing RISs: Enabling dimension-independent CSI acquisition for beamforming," *IEEE Trans. Inf. Theory*, vol. 69, no. 6, pp. 3795–3813, Jun. 2023.

[7] J. Zhu, Z. Gu, Q. Ma, L. Dai, and T. J. Cui, "A self-controlled reconfigurable intelligent surface inspired by optical holography," *Nat. Electron.*, vol. 8, no. 1, pp. 1108–1118, Oct. 2025.

[8] P. Schniter and S. Rangan, "Compressive phase retrieval via generalized approximate message passing," *IEEE Trans. Signal Process.*, vol. 63, no. 4, pp. 1043–1055, Feb. 2015.

[9] Z. Xu, T. Zheng, and L. Dai, "LLM-empowered near-field communications for low-altitude economy," *IEEE Trans. Commun.*, vol. 73, no. 11, pp. 11 186–11 196, Nov. 2025.

[10] J. Vila, P. Schniter, S. Rangan, F. Krzakala, and L. Zdeborová, "Adaptive damping and mean removal for the generalized approximate message passing algorithm," in *Proc. IEEE Int. Conf. on Acoust., Speech and Signal Process. (ICASSP)*, Apr. 2015, pp. 2021–2025.